AIAA JOURNAL
Vol. 46, No. 8, August 2008

Bearing Strength Analysis of Hybrid Titanium Composite Laminates

Jacob M. Hundley,* Jenn-Ming Yang,† and H. Thomas Hahn‡
University of California, Los Angeles, Los Angeles, California 90095
and
Andrew B. Facciano§
Raytheon Missile Systems, Tucson, Arizona 85706

DOI: 10.2514/1.36242

This paper presents a finite element model used to predict the bearing strength of hybrid titanium composite fiber-metal laminates. The model is used to examine the effects of material parameters such as titanium content and edge-distance ratio on specific bearing strength. In addition, a three-dimensional progressive failure user material subroutine is implemented into the commercial finite element code ABAQUS to model stiffness degradation in the graphite–polyimide layers of the hybrid laminate. These results are used to optimize the fiber-metal laminate layup by determining to the ideal tradeoff between joint strength and structural weight.

Nomenclature

C_D	=	degraded stiffness matrix
C_{UD}	=	undamaged material stiffness matrix
D	=	hole diameter
E_L	=	characteristic element length
E_{11}	=	composite modulus along the fiber axis
E_{22}	=	composite modulus transverse to the fiber axis
f_{fc}	=	Hashin fiber compression failure initiation
f_{ft}	=	Hashin fiber tension failure initiation
f_{mc}	=	Hashin matrix compression failure initiation
f_{mt}	=	Hashin matrix tension failure initiation
G_f	=	fiber fracture energy
G_m	=	matrix fracture energy
G_{12}	=	shear modulus fiber–matrix direction
G_{23}	=	shear modulus for the matrix–matrix direction
h	=	laminate thickness
J	=	material Jacobian
P_b	=	bearing load
S_{lt}	=	shear strength for a unidirectional lamina
S_{UD}	=	undamaged material compliance matrix
t	=	pseudotime value at the current finite element analysis increment
$u^{(i)}$	=	displacement measured at node (i)
υ_{12}	=	Poisson's ratio for the fiber–matrix direction
υ_{23}	=	Poisson's ratio for the matrix–matrix direction
w_{fc}	=	degradation variable for the fiber compression failure mode
w_{ft}	=	degradation variable for the fiber tension failure mode
w_{mc}	=	degradation variable for the matrix compression failure mode
w_{mt}	=	degradation variable for the matrix tension failure mode
X_c	=	compressive strength in the fiber direction for a unidirectional lamina
X_t	=	tensile strength in the fiber direction for a unidirectional lamina
Y_c	=	compressive strength transverse to the fiber direction for a unidirectional lamina
Y_t	=	tensile strength transverse to the fiber direction for a unidirectional lamina
Δt	=	difference between successive pseudotime increments
$\Delta\varepsilon$	=	differential strain change between increments
ε_{ij}	=	strain state
$\varepsilon_{ij+}^{\mathrm{init}}$	=	tensile strain component at failure
$\varepsilon_{ij-}^{\mathrm{init}}$	=	compressive strain component at failure
σ_b	=	bearing stress
σ_{ij}	=	stress state
σ_{ys}	=	yield strength

Received 18 December 2007; revision received 25 March 2008; accepted for publication 26 March 2008.

*Graduate Student, Mechanical and Aerospace Engineering Department, Multifunctional Composites Lab, 420 Westwood Plaza.

†Professor, Materials Science Engineering Department, Multifunctional Composites Lab, 420 Westwood Plaza.

‡Professor, Mechanical and Aerospace Engineering Department, Multifunctional Composites Lab, and Materials Science Engineering Department, 420 Westwood Plaza. Senior Member AIAA.

§Senior Principal Systems Engineer, Advanced Systems Design Department, 1151 E. Hermans Road.

Introduction

FIBER-METAL laminates (FMLs) are a class of hybrid composites which consist of thin metal layers adhesively bonded to polymer-matrix composite laminas. These materials combine the beneficial properties of fiber-reinforced polymers, such as fatigue and corrosion resistance, with the damage tolerance and conductivity of metal, while retaining the structural weight advantages of traditional composites. Because of their promising potential for airframe components, the mechanical properties of commercially available FMLs, such as aramid-reinforced aluminum (ARALL) and glass-reinforced aluminum (GLARE), have been extensively studied [1–6].

The most recent FML design iteration is titanium graphite (TiGr), which can be manufactured using processes similar to traditional composites and possesses increased stiffness and strength compared to ARALL and GLARE. In addition, when the graphite fibers are imbedded in a polyimide matrix, TiGr laminates can be used for high-temperature structural applications, such as airframe materials for high-speed civil transport [3]. To use the unique advantages of TiGr materials, it is necessary to develop methodology to predict their deformation and failure in strength limiting applications, particularly for airframe joints in which bolts or rivets are used.

For joints which incorporate bolts or rivets, the introduction of a fastener hole creates a region of stress concentration within the material which reduces its overall strength [7]. The amount of this strength reduction strongly depends on the constitutive nature of the material and on the edge-distance ratio (e/D). The e/D ratio is defined as the spacing between the center of the fastener hole and the free edge of the joint, divided by the fastener diameter.

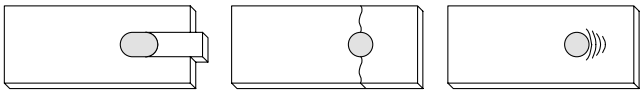

a) b) c)

Fig. 1 Failure modes for bolt loaded joints: a) shearout failure, b) net tension failure, c) bearing failure.

Typical failure modes for a joint loaded in tension are shown in Fig. 1, where shearout and bearing failure represent the lowest and highest strength failure mechanisms, respectively [1]. For composite joints, the failure mode can be directly related to the edge-distance ratio. At small e/D values, the high stress concentration near the hole will cause shearout failure in the composite joint because of the low shear strength of composite materials [8]. As the e/D ratio increases, shear failure of the composite lamina does not propagate to the free edge of the joint and the material fails in a bearing mode. Because the shift from a shearout to a bearing failure mode corresponds to a significant increase in joint strength, the edge-distance ratio corresponding to this failure mode transition is an important quantity in the design of airframe joints. Isotropic or nearly isotropic materials such as aluminum or titanium have a commonly accepted transition point around an edge-distance value of two [9]. Anisotropic materials like polymer-matrix composites have a much higher transition value which depends upon factors such as the fiber orientation and the ratio between the fiber and matrix stiffness properties. Because fiber-metal laminates combine the ductility of a metal with the notch sensitivity of a composite, their transition value is typically between the values of a comparable monolithic metal and a composite-only joint, depending on the volume fraction of the metal within the FML.

To determine the bearing strength of fiber-metal laminate joints, a finite element analysis (FEA) is used to identify the failure mode transition points for a number of edge-distance values as a function of the titanium volume fraction within the TiGr material. A finite element approach is necessary because the three-dimensional stress state which occurs near the hole under bearing-type loading is difficult to predict in closed form unless an infinite plate assumption is used [8]. This assumption is only valid for joints with large edge-distance ratios, making it unsuitable for practical applications in which a large e/D value results in unnecessary structural weight. Additionally, because a finite element analysis breaks the joint into a discrete number of nodes, progressive damage and failure of the composite laminas can be analyzed on a local per-element basis at each integration point. Thus, damage to the composite material can be modeled using only the strength values of its constituents, which reduces the number of experimentally determined parameters required.

In this study, a parameter-based FEA model is used to determine the ultimate bearing strength of an FML joint at several given edge-distance ratios as a function of the titanium volume fraction within the TiGr joint. For each e/D value, the sample layup configurations presented in Table 1 were generated using the following guidelines:

1) The composite laminate must consist of a $[0/\pm 45/90]$ s arrangement, with the titanium plies phased out in a stepwise manner at a distance significantly removed from the joint.

2) The top layer is required to be a 0 deg unidirectional composite lamina.

3) When possible, the titanium layers are separated from one another by the maximum number of composite plies to enhance interlaminar bonding and lap shear strength.

4) When possible, titanium plies are placed between the composite laminas with the largest difference in fiber orientation to reduce residual stresses.

To identify the layup that represents the best design choice for a given edge-distance ratio, the bearing strength data are used to predict the failure mode transition point. These values are presented in specific property form, as a ratio of property to density, to analyze the strength-to-weight benefits of FML joints. Damage visualization and failure of the composite layers are implemented with a three-dimensional progressive damage subroutine which incorporates Hashin's failure criteria [10]. This subroutine expands upon the built-in two-dimensional failure model in the commercial finite element code ABAQUS [11].

Progressive Damage Model

In the majority of finite element studies of the mechanical behavior of composite materials, a plane stress assumption is used to model the composite laminas. Although this assumption is valid in most cases involving laminates loaded in-plane, its utility is limited in applications with a large stress concentration and/or nontrivial through-thickness stress components ($\sigma_{13}, \sigma_{23}, \sigma_{33}$). The bolt hole used to fasten a composite or a fiber-metal laminate joint is a good example of a configuration for which out-of-plane stress terms should be considered. In this case, neglecting these components will significantly overpredict the joint strength. This is due to the fact that the region surrounding the bolt hole is where failure in the joint will occur, regardless of failure mode (Fig. 1). As such, to obtain experimentally reproducible finite element results, it is necessary to first choose an appropriate three-dimensional failure criterion and then implement it in a commercial finite element package.

Constitutive Models for Damaged and Undamaged Laminas

In this study, the Hashin three-dimensional composite failure criterion is used to determine damage initiation within the FML joint. This particular failure criterion was chosen because it has been used successfully in numerous finite element studies of composite materials [1,12–14]. In addition, ABAQUS contains a two-dimensional implementation of Hashin's progressive damage model which can be used for comparison. Expressed in terms of the strain state within the material, four individual failure modes f_i are possible: fiber tension (rupture), fiber compression (buckling), matrix tension (cracking), and matrix compression (crushing). However, at any given point, the compressive and tensile modes for the fiber and matrix are mutually exclusive by definition. It is important to note that the planar failure criterion used in ABAQUS can be derived from Eqs. (1–4) by setting the out-of-plane stress components equal to zero and solving for the strain values. Furthermore, the progressive damage model given in Eqs. (1–13) is intended for use with laminated unidirectional composites and not for woven fabric composites.

Table 1 TiGr layup test matrix

Test matrix no.	Titanium volume, %	Thickness, mm	Layup
1	0.00%	1.016	$[0/-45/45/90]$ s
2	11.50%	1.148	$[0/-45/45/90/\text{Ti}]$ s
3	20.63%	1.280	$[0/-45/\text{Ti}/45/90]$ s
4	28.05%	1.412	$[0/-45/\text{Ti}/45/90/\text{Ti}]$ s
5	34.20%	1.544	$[0/\text{Ti}/-45/45/\text{Ti}/90]$ s
6	39.38%	1.676	$[0/\text{Ti}/-45/45/\text{Ti}/90/\text{Ti}]$ s
7	43.81%	1.808	$[0/\text{Ti}/-45/\text{Ti}/45/\text{Ti}/90]$ s
8	47.63%	1.940	$[0/\text{Ti}/-45/\text{Ti}/45/\text{Ti}/90/\text{Ti}]$ s
9	100.00%	1.016	Monolithic

1) For fiber tension failure mode ($\varepsilon_{11} > 0$)

$$f_{\text{ft}} = \left(\frac{\varepsilon_{11}}{\varepsilon_{11+}^{\text{init}}}\right)^2 + \frac{1}{\varepsilon_{12}^{\text{init2}}}(\varepsilon_{12}^2 + \varepsilon_{13}^2) \geq 1 \tag{1}$$

2) For fiber compression failure mode ($\varepsilon_{11} > 0$)

$$f_{\text{fc}} = \frac{-\varepsilon_{11}}{\varepsilon_{11-}^{\text{init}}} \geq 1 \tag{2}$$

3) For matrix tension failure mode ($\varepsilon_{22} + \varepsilon_{33} > 0$)

$$f_{\text{mt}} = \frac{1}{\varepsilon_{22+}^{\text{init2}}}(\varepsilon_{22} + \varepsilon_{33})^2 + \frac{1}{\varepsilon_{12}^{\text{init2}}}(\varepsilon_{23}^2 + \varepsilon_{12}^2 + \varepsilon_{13}^2 - \varepsilon_{22}\varepsilon_{33}) \geq 1 \tag{3}$$

4) For matrix compression failure mode ($\varepsilon_{22} + \varepsilon_{33} < 0$)

$$f_{\text{mc}} = \frac{1}{\varepsilon_{22-}^{\text{init}}}\left[\left(\frac{\varepsilon_{22-}^{\text{init}}}{2\varepsilon_{12}^{\text{init}}}\right)^2 - 1\right](\varepsilon_{22} + \varepsilon_{33}) + \frac{1}{\varepsilon_{12}^{\text{init2}}}\left[\frac{\varepsilon_{22}^2 + \varepsilon_{33}^2}{2} + \varepsilon_{23}^2 + \varepsilon_{12}^2 + \varepsilon_{13}^2\right] \geq 1 \tag{4}$$

Once damage in the composite layers has been identified using the failure criterion of Eqs. (1–4), the constitutive laws relating the finite element equilibrium strain state to the stress at the current analysis increment must be updated. If the composite lamina is modeled as a transversely isotropic material, then the undamaged stiffness C_{UD} and compliance S_{UD} matrices expressed in reduced index notation are as follows:

$$\mathbf{S}_{\text{UD}} = \begin{bmatrix} 1/E_{11} & -\nu_{12}/E_{11} & -\nu_{12}/E_{11} & 0 & 0 & 0 \\ -\nu_{12}/E_{11} & 1/E_{22} & -\nu_{23}/E_{22} & 0 & 0 & 0 \\ -\nu_{12}/E_{11} & -\nu_{23}/E_{22} & 1/E_{22} & 0 & 0 & 0 \\ 0 & 0 & 0 & 1/G_{12} & 0 & 0 \\ 0 & 0 & 0 & 0 & 1/G_{12} & 0 \\ 0 & 0 & 0 & 0 & 0 & 1/G_{23} \end{bmatrix} \tag{5}$$

$$\mathbf{C}_{\text{UD}} = \mathbf{S}_{\text{UD}}^{-1} \tag{6}$$

Damage that occurs in any of the four aforementioned failure modes will reduce the load-carrying capability of the composite and, therefore, the material stiffness matrix. Using the concept of effective stress area, introduced by Matzenmiller et al., the stiffness matrix is reduced by a degradation factor w_i corresponding to each failure mode, presented in Eqs. (7–10) [15]. The value of this factor depends on the values of the Hashin failure initiation criteria at the given strain state. The degradation variables are derived from the forms presented by Linde et al. and are modified to include all four Hashin failure modes [16]. Each degradation variable has a zero value before damage initiation and increases exponentially to one with increasing Hashin failure initiation value, listed in Eqs. (1–4):

$$w_{\text{ft}} = 1 - (1/f_{\text{ft}})\exp[-C_{\text{UD}}(1,1)(\varepsilon_{11+}^{\text{init}})^2(f_{\text{ft}} - 1)E_L/G_f] \tag{7}$$

$$w_{\text{fc}} = 1 - (1/f_{\text{fc}})\exp[-C_{\text{UD}}(1,1)(\varepsilon_{11-}^{\text{init}})^2(f_{\text{fc}} - 1)E_L/G_f] \tag{8}$$

$$w_{\text{mt}} = 1 - (1/f_{\text{mt}})\exp[-C_{\text{UD}}(2,2)(\varepsilon_{22+}^{\text{init}})^2(f_{\text{mt}} - 1)E_L/G_m] \tag{9}$$

$$w_{\text{mc}} = 1 - (1/f_{\text{mc}})\exp[-C_{\text{UD}}(2,2)(\varepsilon_{22-}^{\text{init}})^2(f_{\text{mc}} - 1)E_L/G_m] \tag{10}$$

Figure 2 shows the relationship between the damage initiation values and the degradation variables for each failure mode. These values were evaluated using experimentally determined material properties of a graphite–polyimide lamina. The degradation curves are contained by a damage control envelope (DCE) defined with an upper bound formed by the Kronecker delta function and a lower bound equal to the degradation variable without the exponential term:

$$\left(1 - \frac{1}{f_i}\right) < \text{DCE} < \delta_{ij} \quad \text{where } i = j \quad \text{if } f_i \geq 1, \quad \text{else } i \neq j \tag{11}$$

Finally, the individual components of the undamaged stiffness matrix are degraded depending on whether their values are derived from the fiber material properties, the matrix material properties, or both. An important feature of the constitutive relation in Eq. (12) is that the transversely isotropic nature of the material is retained following damage initiation and progression.

$$\mathbf{C}_{\text{UD}} = \begin{bmatrix} d_{11}C_{\text{UD}}(1,1) & d_{12}C_{\text{UD}}(1,2) & d_{12}C_{\text{UD}}(1,2) & 0 & 0 & 0 \\ d_{12}C_{\text{UD}}(1,2) & d_{22}C_{\text{UD}}(2,2) & d_{22}C_{\text{UD}}(2,3) & 0 & 0 & 0 \\ d_{12}C_{\text{UD}}(1,2) & d_{22}C_{\text{UD}}(2,3) & d_{22}C_{\text{UD}}(2,2) & 0 & 0 & 0 \\ 0 & 0 & 0 & d_{12}C_{\text{UD}}(4,4) & 0 & 0 \\ 0 & 0 & 0 & 0 & d_{12}C_{\text{UD}}(4,4) & 0 \\ 0 & 0 & 0 & 0 & 0 & d_{22}C_{\text{UD}}(6,6) \end{bmatrix} \tag{12}$$

$$d_{ij} = \begin{bmatrix} d_{11} = (1 - w_{\text{ft}})(1 - w_{\text{fc}}) \\ d_{12} = (1 - w_{\text{ft}})(1 - w_{\text{fc}})(1 - w_{\text{mt}})(1 - w_{\text{mc}}) \\ d_{22} = (1 - w_{\text{mt}})(1 - w_{\text{mc}}) \end{bmatrix} \tag{13}$$

Solution Convergence and the Material Jacobian

Equation (12) represents the degraded material stiffness matrix, which is used to define the constitutive relations of the composite lamina following damage initiation. It is also used in the finite

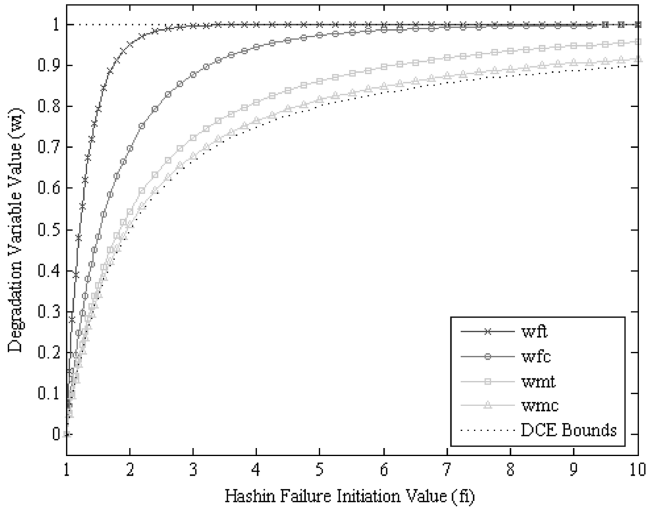

Fig. 2 Degradation variables as a function of Hashin's failure initiation criteria [16].

element implementation to check for solution convergence via the tangent stiffness matrix. Defined as the derivative of a change in a given component of the stress tensor with respect to a change in a given strain tensor component, the tangent stiffness matrix is used in an implicit finite element analysis to produce a first guess for the iterative solution method at successive steps in the analysis. The tangent stiffness is particularly important for the progressive damage methodology outlined in Eqs. (1–13) because the constitutive relations for the composite laminas exhibit significant strain softening upon damage initiation. This nonlinear material behavior can lead to stability and convergence issues in the model if the finite element equation solver does not begin with a good guess at the start of the analysis increment. From the preceding definition, the tangent stiffness matrix can be derived from the two-dimensional form employed by ABAQUS using the strain dependence of Eqs. (1–13). From standard constitutive theory, the instantaneous stiffness matrix C is defined from the incremental stress-strain relation as:

$$\Delta\vec{\sigma} = \mathbf{C}\Delta\vec{\varepsilon} \tag{14}$$

If progressive damage in the composite lamina is not considered, then the change in the stress state of Eq. (14), resulting from a differential increase in strain, can be evaluated directly using the constant undamaged stiffness matrix C_{UD}. This illustrates that, before damage initiation, the tangent and undamaged stiffness matrices are identical, which is expected for a linear analysis. However, if progressive damage is implemented, then the stiffness matrix components contain degradation variables, as shown in Eq. (12). In this case, it is important to note that the instantaneous stiffness matrix $C(\varepsilon)$ is an implicit function of strain. Therefore, as the strain is increased by this differential amount $\Delta\varepsilon$, the tangent stiffness can be obtained from

$$\mathbf{C}(\vec{\varepsilon} + \Delta\vec{\varepsilon}) = \mathbf{C} + \frac{\partial \mathbf{C}}{\partial \vec{\varepsilon}}\Delta\vec{\varepsilon} \tag{15}$$

In the preceding equation, the derivative of the instantaneous stiffness matrix with respect to the incremental strain state is herein defined as the material Jacobian J. Because the stiffness matrix is a function of all four degradation variables, Eq. (15) can be expanded to include all four failure modes.

$$\mathbf{J} = \frac{\partial \mathbf{C}}{\partial \vec{\varepsilon}} = \sum_{i=1}^{4}\left[\left(\frac{\partial \mathbf{C}}{\partial w_i}\right)\left(\frac{\partial w_i}{\partial \vec{\varepsilon}}\right)\right] \tag{16}$$

From the degradation variable forms of Eqs. (7–10), all of the quantities in their expressions are strain-state independent except for the Hashin failure initiation values, Eqs. (1–4), which also depend on the strain value at the current increment. Therefore, the tangent stiffness matrix is equal to the degraded stiffness matrix plus a series of additional terms, shown in Eq. (17). These terms account for the dependence of the constitutive relations on the current strain state, introduced with the incorporation of progressive damage within the material.

$$\mathbf{J} = \sum_{i=1}^{4}\sum_{j=1}^{4}\left[\left(\frac{\partial \mathbf{C}_D}{\partial w_i}\right)\left(\frac{\partial w_i}{\partial f_j}\right)\left(\frac{\partial f_j}{\partial \vec{\varepsilon}}\right)\right] \tag{17}$$

Implementation of the methodology presented in the preceding section into a FORTRAN script follows the flowchart of Fig. 3. History-dependent quantities, such as the stress and strain state, failure initiation values, and degradation variables, are passed back to ABAQUS for storage and indexing at later increments. Array quantities such as the stiffness and compliance matrices, as well as the material Jacobian, are calculated at each increment and not returned to the ABAQUS processor. Recalculating these values at each increment did not significantly impact program runtime and reduced the storage requirements on ABAQUS, because the material Jacobian is nonsymmetric and contains 36 independent quantities.

Finite Element Modeling

Model Parameters

The finite element simulation results presented in this study use both the titanium volume fraction of the fiber-metal laminates and the edge-distance ratio of the specimen as parameters. The geometry of the FML model used in the finite element simulations is similar to that specified in ASTM D953 and ASTM D5961 with a 3-in. straight-sided gauge region and a bolt hole of diameter 0.25 in. [17,18]. Figure 4 shows the three-dimensional geometry of the FML, where the overall model thickness depends on the particular layup, outlined in Table 1. Each layer was modeled using three-dimensional linear reduced integration elements, denoted C3D8R in ABAQUS. Because continuum shell elements were not used for the composite layers, additional degrees of freedom were possible within the model. This allowed the composite laminas to carry through-thickness stress components essential to monitoring three-dimensional progressive damage. The titanium layers were assumed to be linear elastic with an isotropic plastic hardening region following the yield point, determined from experimental testing of a uniaxial tension specimen. The graphite–polyimide composite layers were modeled with a user material subroutine (UMAT), which incorporates the stiffness degradation presented previously. The UMAT was called at each integration point in the composite material at every increment, and fits into the ABAQUS processor as shown in Fig. 5.

To accurately replicate the bolt-type bearing test procedure, a fixed grip boundary condition was imposed at the unnotched end of the gauge region. This was done by setting all planar degrees of freedom to zero, consistent with a perfect grip assumption. Additionally, symmetry boundary conditions were used to eliminate redundant calculations and improve simulation runtime. Because each layup in Table 1 is symmetric about the midplane, only one-half of the FML thickness was modeled, whereas symmetry about the plane of the applied load allows for half of the laminate width to be modeled. Figure 4 displays the explicitly stated boundary conditions on the completed model. Additional implicit boundary conditions were imposed upon the model by incorporating a rigid backing plate, which is assumed to be perfectly clamped to the specimen. The perfect clamping assumption implies that zero fastener torque is initially present in the model. This represents a slight departure from the 2.2–3.4 N · m torque specified in ASTM D5961, but is still within the range of allowable variations, and represents a "finger-tightened" joint [18]. The backing plate resists positive out-of-plane deformation of the material which results from delamination of the composite layers in the pin contact region. Because the clamping force provided by the backing plate resists delamination, cohesive elements were not required between each layer. This is not to say that delamination does not occur, rather that it is not included in the finite

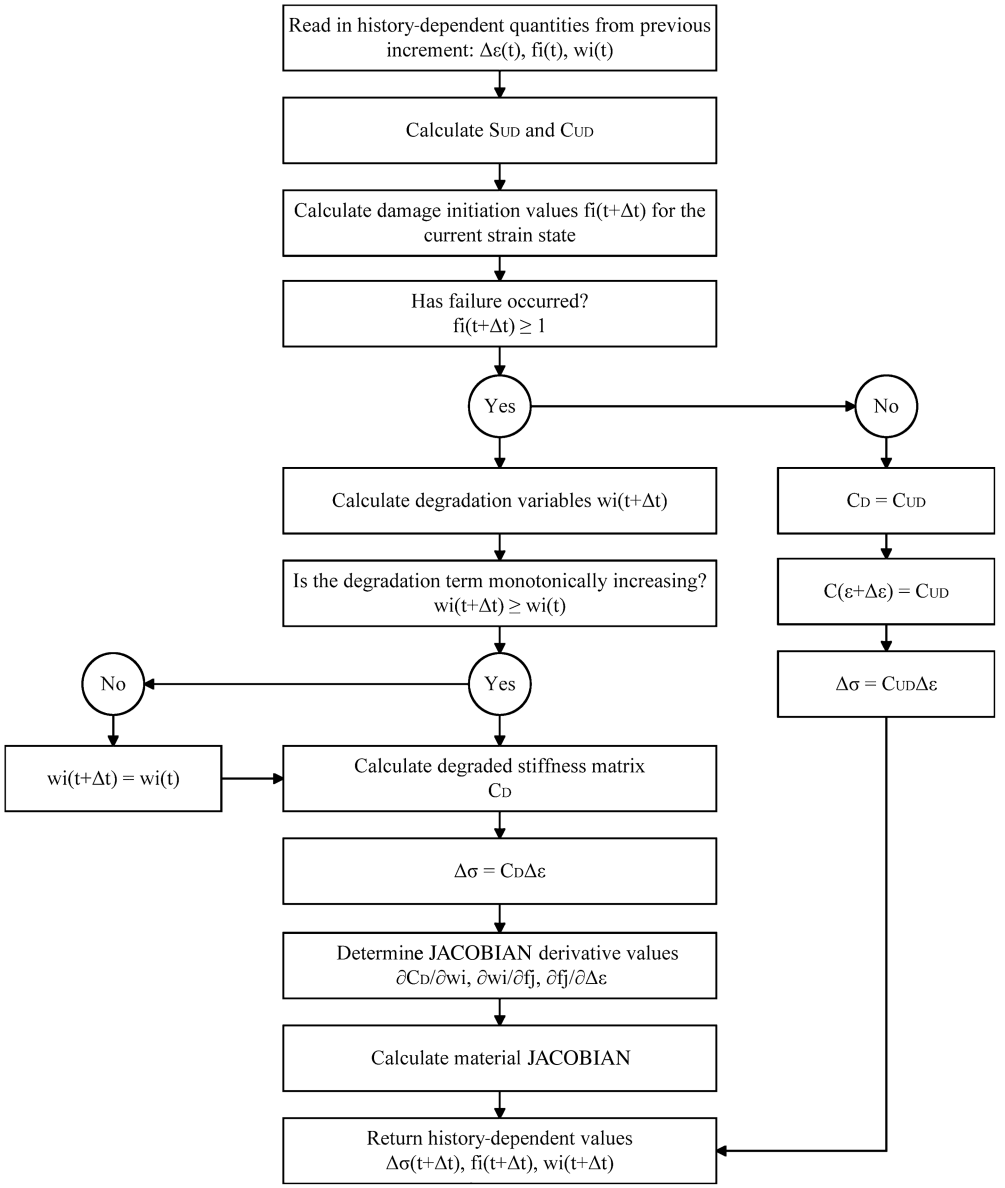

Fig. 3 Flowchart for numerical implementation of progressive damage.

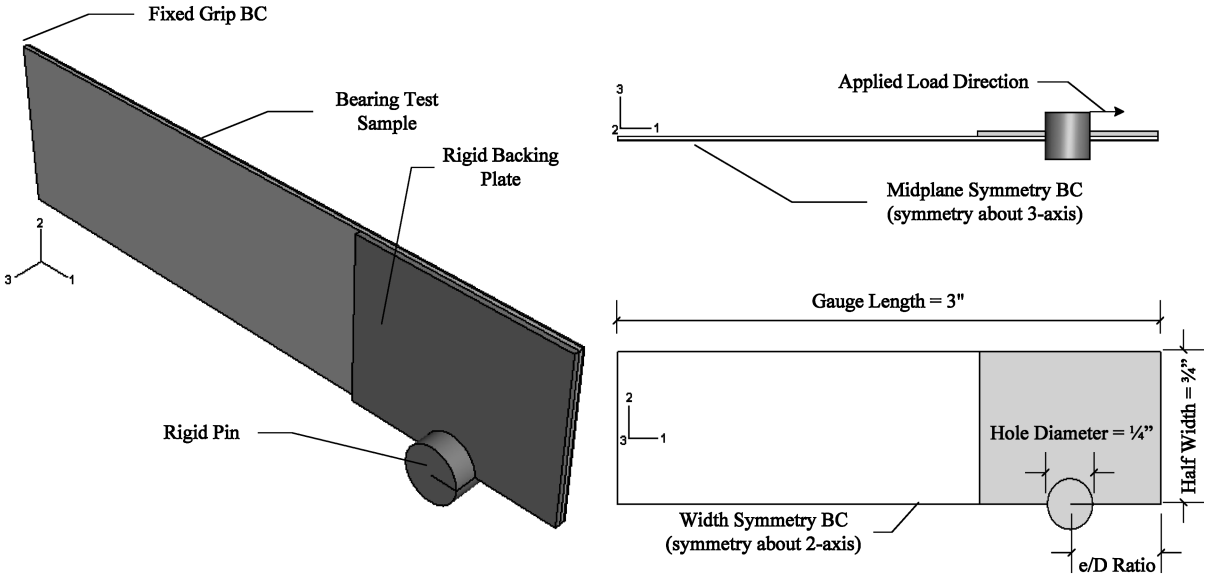

Fig. 4 Finite element model geometry and boundary conditions.

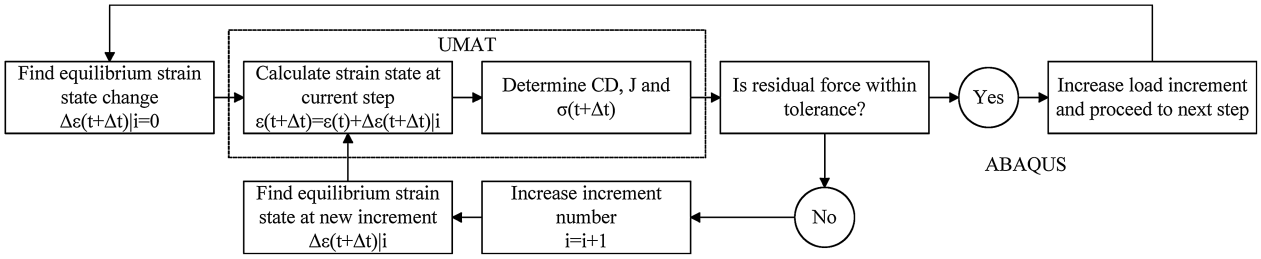

Fig. 5 Positioning of the UMAT subroutine within the ABAQUS processor.

element model to vastly increase computational efficiency when user-defined material nonlinearity is present. Although delamination formation and propagation do impact the joint strength and failure mode, it is common practice to neglect these effects if out-of-plane displacement constraints are used [1]. Therefore, the degrees of freedom at the surface of each layer were tied to those of the adjacent layer, which is the result of a perfect interfacial bonding assumption. The motion of the backing plate was fixed to the pin through a nodal coupling constraint, and tangential friction between the plate and the top layer of the FML was used in the model. The pin itself was assumed to be perfectly rigid because it has a much higher stiffness than the fiber-metal laminate. The pin was constrained to move only along the direction of the applied load, corresponding to the motion of the crosshead in a bolt-type bearing test. The bearing stress applied to the FML sample, which separates each load increment in the finite element (FE) simulations, was calculated from the pin load applied P, as per Eq. (18). It is important to note that this bearing stress value is one-quarter of that of ASTM D953 because of the symmetry boundary conditions present in the model [17].

$$\sigma_b = \frac{P_b}{Dt} \quad \text{where } P_{\text{FEM}} = \frac{P_b}{4} \tag{18}$$

due to symmetry boundary conditions (BCs).

The finite element mesh used to discretize the geometry of Fig. 4 is broken into three distinct regions of refinement. These regions are referred to as the high, medium, and low refinement zones. Each region is distinguished by its probability of damage initiation, with more elements corresponding to a region of higher damage probability. Examples of the mesh geometry are shown in Fig. 6 for e/D ratios of 1.0 and 2.5.

Data Acquisition and Measurement

At each load increment, a set of state dependent FML quantities were stored by ABAQUS and used in the postprocessing analysis. The most important of these are the Hashin failure initiation value of Eqs. (1–4). These values are used to track the history-dependent damage progression in the material and identify the bearing failure mode. The hole deformation percentage was determined using the displacement of a simulated nodal strain gauge. The gauge consisted of the node at the pin contact point and a second node spaced by approximately 3 cm along the width symmetry axis, as shown in Figs. 6a and 6b. The hole deformation at a given increment was then calculated using the current displacement of the nodes and the original spacing of the simulated strain gauge:

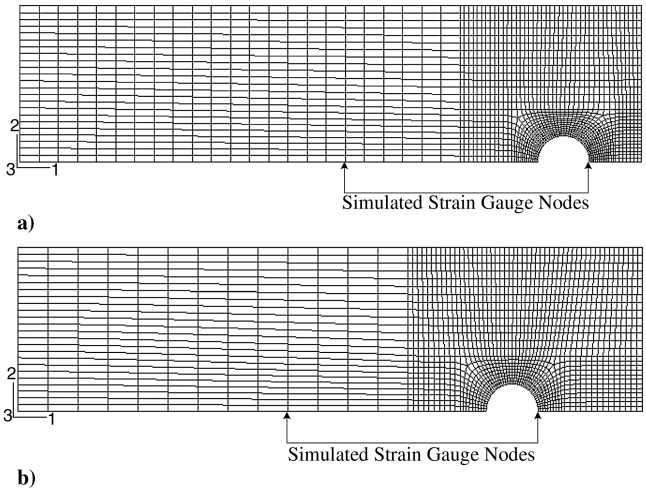

Fig. 6 Sample finite element meshes for e/D ratios of a) 1.0 and b) 2.5.

$$\text{hole deformation} = \frac{u^{(1)}(t+\Delta t) - u^{(2)}(t+\Delta t)}{D(t=0)} \cdot 100\% \tag{19}$$

Results

Finite Element Bolt-Bearing Model Validation

Because experimental results for the TiGr FML samples were not available, the finite element bearing strength data were compared with existing literature values to validate the accuracy of the calculations. Validation of the bolt-bearing model parameters was performed using a seven-factor Taguchi test matrix (Table 2). This matrix was used to investigate the effects of user-defined finite element input values on the measured bearing strength. The Taguchi results were compared with the experimentally determined bearing strength of aluminum from a materials handbook in all eight cases [9]. The final model listed in Table 2 was obtained through statistical analysis of these results, which provided the relative impact of the parameters upon the calculated bearing strength. The bearing strength of an aluminum finite element model with these parameters, and material properties listed in Tables 3 and 4, was 1.89% higher than the experimentally measured data, which constitutes a good approximation.

Table 2 Parameter validation Taguchi test matrix

Test no.	Bolt hole mesh refinement	Element type	Metal model	Hole tolerance	Pin tolerance	Pin-sample friction	Out-of-plane BCs
1	100 nodes	C3D8R	Isotropic plasticity	0%	0%	0.05	Rigid backing constraint
2	100 nodes	C3D8R	Isotropic plasticity	+2%	−2%	0.25	Applied pressure
3	100 nodes	C3D8	Trilinear elasticity [1]	0%	0%	0.25	Applied pressure
4	100 nodes	C3D8	Trilinear elasticity [1]	+2%	−2%	0.05	Rigid backing constraint
5	200 nodes	C3D8R	Trilinear elasticity [1]	0%	−2%	0.05	Applied pressure
6	200 nodes	C3D8R	Trilinear elasticity [1]	+2%	0%	0.25	Rigid backing constraint
7	200 nodes	C3D8	Trilinear elasticity [1]	0%	−2%	0.25	Rigid backing constraint
8	200 nodes	C3D8	Isotropic plasticity	+2%	0%	0.05	Applied pressure
Final	100 nodes	C3D8R	Isotropic plasticity	+1%	0%	0.10	Rigid backing constraint

Table 3 Material properties used in the finite element model

Material	Parameter values, GPa					
	E_{11}	E_{22}	G_{12}	G_{23}	v_{12}	v_{23}
Al 2024-T3 [10]	72.40	72.40	27.61	27.61	0.33	0.33
S2 glass [1]	53.98	9.41	2.70	3.00	0.33	0.33
Ti 4V-6Al [10]	107.20	107.20	40.30	40.30	0.33	0.33
Graphite-polyimide	151.69	6.90	2.41	3.22	0.30	0.46

Table 4 Damage and failure properties used in the finite element model

Material	Parameter values, MPa					
	σ_{ys}	X_t	X_c	Y_t	Y_c	S_{lt}
Al 2024-T3 [10]	350.00	——	——	——	——	——
S2 glass [1]	——	2429.00	2429.00	68.00	68.00	75.00
Ti 4V-6Al [10]	888.20	——	——	——	——	——
Graphite-polyimide	——	2068.50	413.70	13.79	68.95	27.58

In addition, the fiber-metal laminate model values were verified by replicating the experimental results presented by Van Rooijen et al. [1]. A good correlation was obtained between the GLARE 2 experimental data and the finite element results, as presented in Fig. 7. The FE simulation error values for the bearing ultimate strength were between −7.49 and 2.99%, where the sign of the simulation error was seen to change from positive to negative at an edge-distance ratio of two. This shift in error values corresponds to a change in the failure mode of the laminate, from shearout to bearing-type failure. Net tension type failure, Fig. 1b, did not occur for any of the FML specimens in this study because the joint width is large compared to the fastener diameter. The simulation error values suggest that the finite element model overestimates the joint strength for shearout failure and underestimates the strength for bearing failure. It should be noted that for bolt-type bearing, failure of the joint is due to local instability and not fracture, as is the case for a shearout-type failure. From the model outlined in Fig. 4, the failure stress in a bearing failure mode is defined as the first discontinuity due to local fiber buckling in the pin force vs displacement curve. This definition is overly conservative; local discontinuities can be mistaken for mechanical vibrations during testing, and local buckling does not result in a full reduction of the joint bearing capabilities. Therefore, the slightly higher error values for bearing-type failure can be explained by the ambiguity in the failure definition. However, both error values are well within an acceptable tolerance level and a certain amount of simulation error is to be expected due to the natural variability of composite materials.

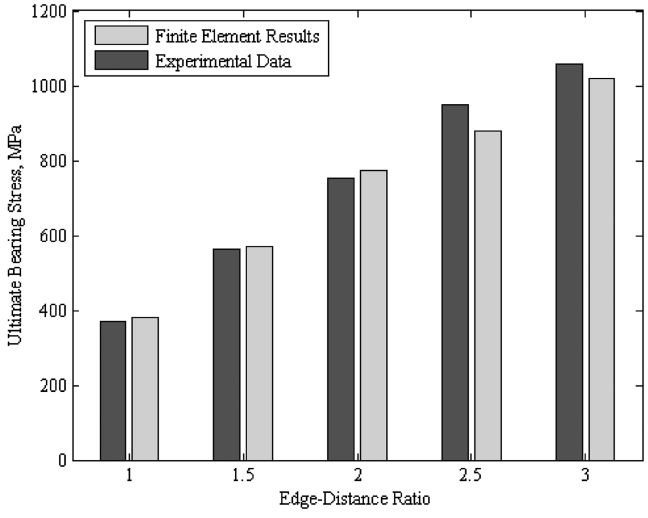

Fig. 7 Finite element comparison with experimental data for GLARE 2 [1].

Two- and Three-Dimensional Failure Criterion Comparison

To obtain experimentally reproducible FE strength results, it is essential to correctly identify damage initiation within the composite layers. As shown in Eq. (12), nonlinearity in the composite constitutive relations will significantly affect deformation of the joint. Therefore, the stress at which this nonlinearity occurs and, by association, the failure criterion used are of critical import in the analysis. The necessity of a three-dimensional failure model is evident from existing fiber-metal laminate literature. Van Rooijen et al. studied the bearing strength of GLARE laminates and concluded that the error in finite element calculations using a two-dimensional failure model is most likely due to underestimation of fiber damage within the glass-epoxy layers [1]. The difference in stiffness degradation between two- and three-dimensional failure initiation values can be visualized using the history-dependent failure values stored in ABAQUS. Figure 8 shows the FML Hashin failure results f_i in composite layers with different fiber orientations at an edge-distance ratio of two. In the figure, the finite element results in Figs. 8a–8c represent the built-in ABAQUS damage model, whereas the images in Figs. 8d–8f were generated with the three-dimensional failure subroutine outlined previously. For both models, a state variable value greater than or equal to one corresponds to a point at which the failure criteria value has been exceeded, indicating that damage has occurred in the given mode. In each case, the shape of the damage envelope is similar, but the three-dimensional model clearly identifies damage initiation at a greater number of integration points for each sample.

As seen in Fig. 8, the inability of the finite element model to properly detect damage can be attributed to neglecting the out-of-plane components in the Hashin failure criterion. For a bolt-type bearing model, the plane stress assumption associated with a two-dimensional failure criterion is only applicable for points in the gauge region of the sample. This result is evident from Figs. 9 and 10 which show the ratio between the in-plane and out-of-plane strain terms expressed as a percentage for a $[0/-45/\mathrm{Ti}/45/90]$ s titanium-graphite fiber-metal laminate. Figure 9 displays the strain ratios measured from the bolt hole to the clamped end of the gauge section, whereas Fig. 10 shows strain ratios measured from the bolt hole to the free edge of the sample. In the figures, the through-thickness strain values are of the same order of magnitude as the planar values at nodes located near the hole. Examining Fig. 9 in particular shows that, near the bolt hole, the out-of-plane normal strain (ε_{33}) is 3.16 and 8.97 times larger than both in-plane normal strains ($\varepsilon_{11}, \varepsilon_{22}$), respectively. Additionally, the out-of-plane shear component (ε_{13}) is 5.59 times greater than the planar shear term (ε_{12}). This same result applies for nodes located at the other end of the bolt hole, as evidenced by Fig. 10. These significant increases can be attributed to the boundary conditions applied by the rigid pin and backing plate. Because of the high stress level resulting from the point loads applied by the pin in the contact region, the material's natural response is to deform in a direction orthogonal to the load application path, resulting in delamination. However, the clamping force provided by the backing plate resists delamination by limiting the out-of-plane deformation of the sample. As a result, a large through-thickness strain state occurs as the material is crushed between the two rigid bodies.

Because the through-thickness strain values are not trivial, as assumed with a planar model, the Hashin failure initiation terms in Eqs. (1–4) approach unity much faster when three-dimensional components are included. Thus, stiffness degradation occurs at lower stress levels. In Figs. 11a and 11b, the ratios of out-of-plane to in-plane strain components as a function of bearing stress are shown for a node located at 90 deg with respect to the load applied direction for edge-distance ratios of 0.75 and 3.0, respectively. These results show that all of the through-thickness strain components must be included in the failure criterion, because the dominant out-of-plane strain term will change as a function of applied bearing stress and edge-distance ratio. Even though this effect is localized in the bolt-hole vicinity, it greatly affects the measured finite element strength because the region surrounding the hole is where the joint will fail, regardless of bearing failure mode. At distances sufficiently removed from the bolt

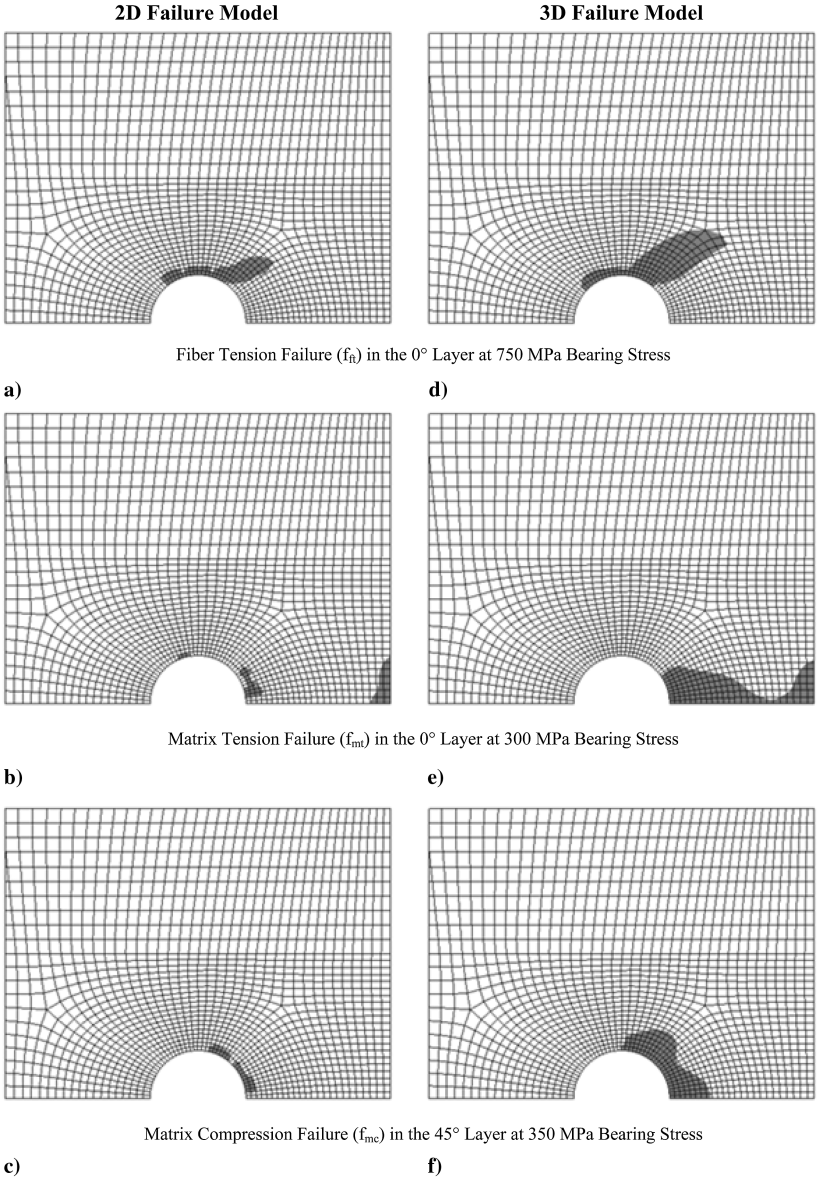

Fig. 8 Failure mode comparison for two- and three-dimensional models. Common contour scale, shaded areas represent Gauss points at which the failure criteria have been exceeded.

hole, the planar terms dominate and the through-thickness stress and strain components can be neglected. At these nodes, failure initiation and damage progression is still modeled using the Hashin three-dimensional criterion, however, because the gauge region in the finite element model is small and implementation of the failure subroutine does not significantly impact simulation runtime. For systems with large numbers of degrees of freedom, a two-dimensional failure model can be implemented in regions sufficiently removed from the bolt hole, although more research is necessary to determine this distance.

Bearing Strength as a Function of Edge-Distance Ratio and Titanium Content

For each layup listed in Table 1, the ultimate bearing strength was determined using the three-dimensional failure constitutive model, Eq. (12), for edge-distance ratios of 0.75, 1.0, 1.5, 2.0, 2.5, and 3.0. The finite element results are summarized in Table 5, which provides the percentage increase in the maximum pin load at failure, Eq. (18), of a fiber-metal laminate joint compared to a composite-only joint. Additionally, to offset the strengthening effects due to increased thickness of the laminate, the bearing strength values are represented in specific property form in Fig. 12. It should be noted here that, in the optimization of titanium-graphite fiber-metal laminate joints, ultimate strength is not the only parameter to consider. However, because joint strength is the parameter of interest in this study, and the constitutive model presented in Eqs. (1–13) is validated in terms of ultimate strength, Table 5 and Fig. 12 are useful in the strength-optimized design of titanium-graphite joints. From Fig. 12, it is clear that the specific bearing strength increases with higher edge-distance ratios. This result is to be expected because the added material between the bolt hole and the free edge of the joint provides reinforcement by moving the region of stress concentration away from the joint edge. In particular, because graphite–polyimide composites have a high level of notch sensitivity, this reinforcement effect can be seen at small edge-distance values for fiber-metal laminates with low metal volume fractions. At the transition from edge-distance values of 0.75–1.0, Fig. 12 shows that the relative strengthening effect due to the increased edge-distance decreases as a function of titanium volume fraction. Specifically, increasing the edge-distance value by 0.25 results in a 34.8% increase in bearing strength for the composite-only joint compared with a 27.3% improvement for a TiGr sample with 47.6% titanium.

In addition, Fig. 12 shows that the relationship between specific strength and titanium content is a function of the e/D ratio. In other words, the difference in strength associated with adding or

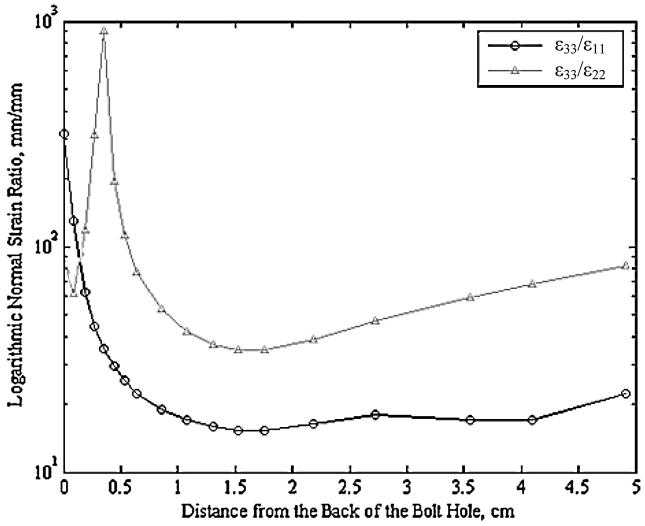

a)

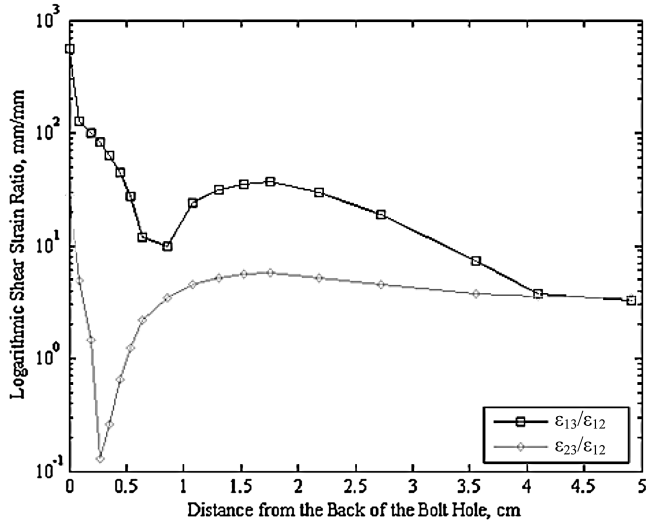

b)

Fig. 9 Ratio of out-of-plane to in-plane strains at the joint centerline in a direction opposite the applied load for a [0/ − 45/Ti/45/90] s TiGr laminate: a) normal strain, b) shear strain.

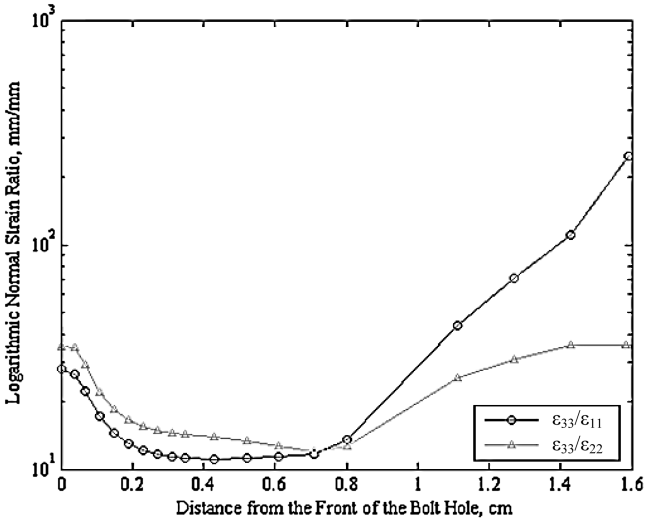

a)

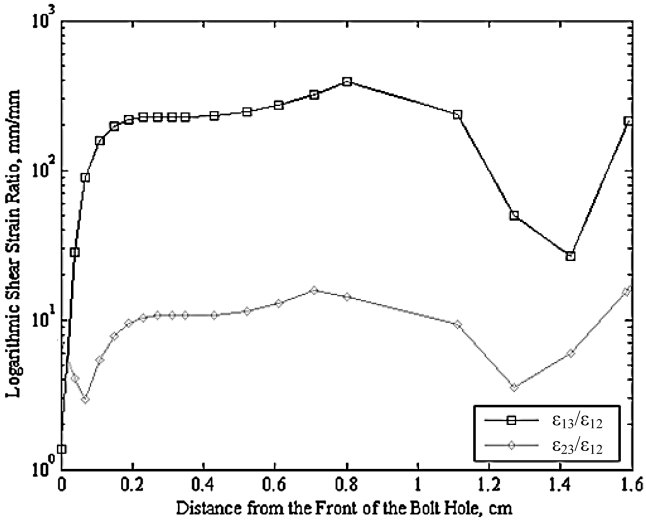

b)

Fig. 10 Ratio of out-of-plane to in-plane strains at the joint centerline in the direction of the applied load for a [0/ − 45/Ti/45/90] s TiGr laminate: a) normal strain, b) shear strain.

subtracting titanium plies depends on the joint geometry. Essentially, the specific bearing strength to volume fraction chart can be broken down into three regions dependent upon this correlation: a low region ($e/D \leq 1.0$), a medium region ($1.0 < e/D < 3.0$), and a high region ($e/D \geq 3.0$). In the low region, the relationship between specific bearing strength and volume fraction is nearly linear and the strength decreases monotonically with increasing titanium content. This linear relation is due to the fact that, at low e/D ratios, all of the joints fail in a shearout mode, regardless of their titanium content. Figure 13a displays an example of damage progression leading to shearout failure in a fiber-metal laminate joint with an edge-distance ratio of 0.75. Although the monolithic metal and TiGr samples fail at higher stress levels, their additional structural weight results in lower specific strength. This effect is naturally more pronounced at higher titanium content values. As a consequence, for e/D values less than one, low titanium volume fraction TiGr layups are optimal configurations because they improve joint strength without a significant weight penalty. For example, at an edge-distance ratio equal to 0.75, replacing the composite-only joint in Fig. 4 with a 20.6% titanium content TiGr joint of identical geometry produces a 24.8% gain in bearing strength.

In the medium region, at edge-distance values greater than one, the specific bearing strength to titanium volume fraction curve becomes nonlinear. In this case, the composite-only and TiGr joints remain in a shearout failure mode, whereas the metal joint mode shifts from shearout to bearing. From Table 4 and Fig. 12, the TiGr joints show increased strength compared with the composite joints, yet their specific property values do not greatly improve because they remain in the strength limiting shearout failure mode. Therefore, there is no optimum layup configuration in the medium edge-distance region.

The most important conclusion that is drawn from the specific strength chart is that a transition from shearout to bearing failure, shown in Fig. 13b, occurs in TiGr joints with titanium volume fractions on the order of 40–50% for edge-distance ratios near three. Bearing failure occurs primarily due to fiber buckling and local instability ahead of the pin contact region, as shown in Fig. 13b, and is also attributable to transverse and shear cracking in the polymer matrix. The change in failure modes in the high-e/D region corresponds to a huge bearing strength improvement, which completely offsets the weight increase associated with the addition of titanium plies. For these configurations, the titanium layers undergo significant plastic deformation which reduces the notch sensitivity of the fiber-metal laminate. As a result, fiber tensile damage is contained in the area surrounding the bolt hole and does not propagate to the free edge of the specimen, preventing failure in the shearout mode. The same result can be obtained for TiGr joints with lower titanium content simply by raising the edge-distance ratio, although, for layups with a small number of titanium plies, the transition occurs at

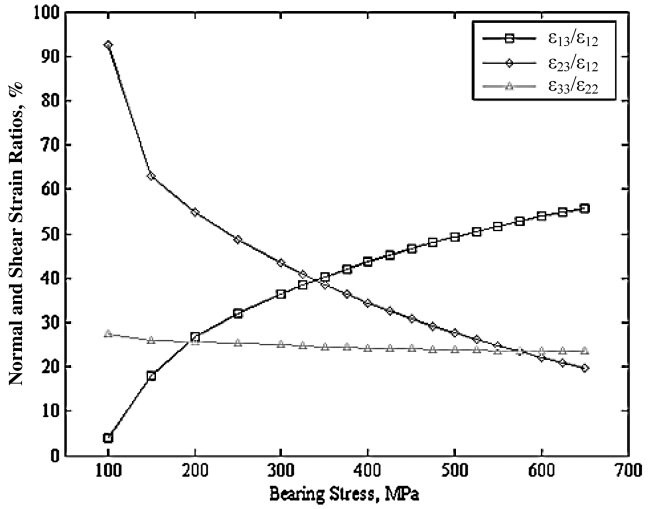

a)

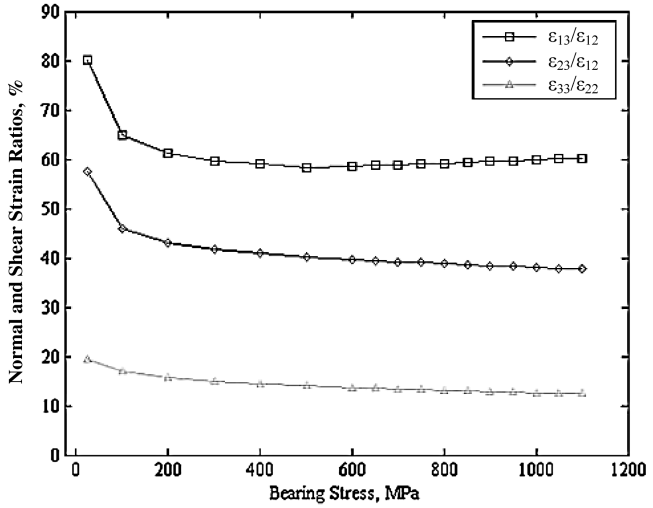

b)

Fig. 11 Bearing stress vs the ratio of out-of-plane to in-plane strain components at a node oriented at 90 deg with respect to the load applied direction for a [0/ − 45/Ti/45/90] s TiGr laminate: a) $e/D = 0.75$, b) $e/D = 3.0$.

e/D values which are too large to be used in practical applications. Figure 14 shows the relationship between titanium volume fraction and the edge-distance ratio required for the joint to fail in a bearing mode. From this chart, it is apparent that the optimum TiGr layup for a structural component in the high-e/D region depends entirely upon the edge-distance value. As stated earlier, bearing-type failure represents the highest strength failure mode in the joint. Therefore, if the e/D ratio of an airframe component is known, then the curve presented in Fig. 14 will predict the mode in which the TiGr layups in Table 1 will fail. This information can be used to determine the optimal joint configuration, which corresponds to the layup with the

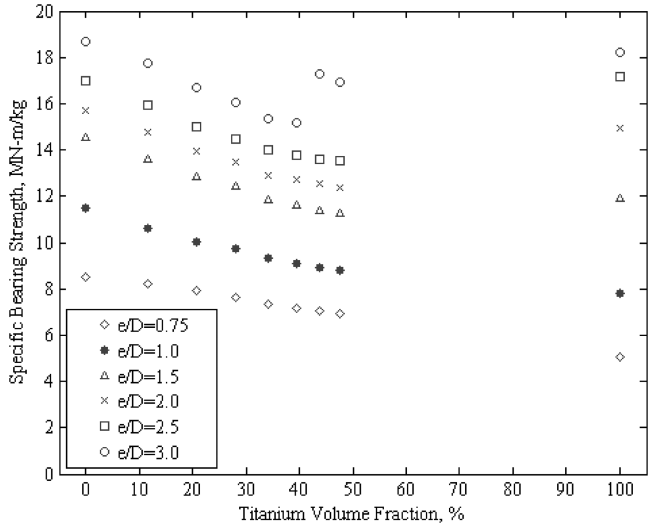

Fig. 12 Predicted specific bearing strength as a function of edge-distance ratio.

smallest titanium volume fraction that fails in a bearing mode. For example, at an e/D value of three, the best layup choice from Table 1 would be a 43.8% titanium volume fraction FML, which corresponds to the most ideal tradeoff between joint strength and weight.

Conclusions

The results presented in this study show that a finite element model is capable of predicting the bolt-type bearing behavior for both monolithic metal and fiber-metal laminate joints. In addition, results show that composite laminas, modeled with three-dimensional stress elements and a progressive failure constitutive model, predict damage onset and nonlinear behavior at lower bearing stress levels when compared with the built-in ABAQUS planar failure model. The necessity of this three-dimensional model is apparent from the nontrivial out-of-plane strain state which exists around the bolt hole, and also from existing fiber-metal laminate literature.

Use of this finite element model to determine the ultimate bearing strength of titanium-graphite fiber-metal laminates showed that the relationship between joint strength improvement and increasing titanium volume fraction is dependent upon the edge-distance ratio. In particular, three distinct edge-distance regions were identified, each corresponding to its predominant bearing failure mode. At edge-distance values between 0.75 and 1.0, all of the laminates were seen to fail in a shearout mode, regardless of titanium volume fraction. In this case, fiber-metal laminate joints with titanium content between 10 and 21% represent the optimum layups, as they improve the joint bearing strength without significantly impacting the structural weight. For edge-distance values greater than 1.0, but less than 3.0, the fiber-metal laminate joints still showed improvement over a composite-only joint, but no optimum layup exists because each TiGr laminate remains in a shearout failure mode. Finally, at edge-distance ratios greater than 3.0, a failure mode transition from shearout to bearing failure occurs for laminates with

Table 5 Predicted percentage increase in pin force at failure for FML vs composite joints

Titanium volume fraction	Increase in maximum applied pin force P over a composite-only joint, %					
	$e/D = 0.75$	$e/D = 1.00$	$e/D = 1.50$	$e/D = 2.00$	$e/D = 2.50$	$e/D = 3.00$
11.50%	29.67%	24.66%	25.69%	26.46%	26.39%	27.74%
20.63%	57.22%	47.85%	49.17%	50.12%	49.71%	51.21%
28.05%	83.11%	73.15%	74.06%	74.82%	73.87%	74.91%
34.20%	105.73%	94.04%	96.04%	95.75%	96.48%	95.69%
39.38%	129.29%	117.11%	117.89%	120.69%	121.79%	121.83%
43.81%	154.78%	139.35%	141.13%	145.59%	146.21%	184.41%
47.63%	178.71%	163.14%	164.65%	170.15%	172.44%	210.50%

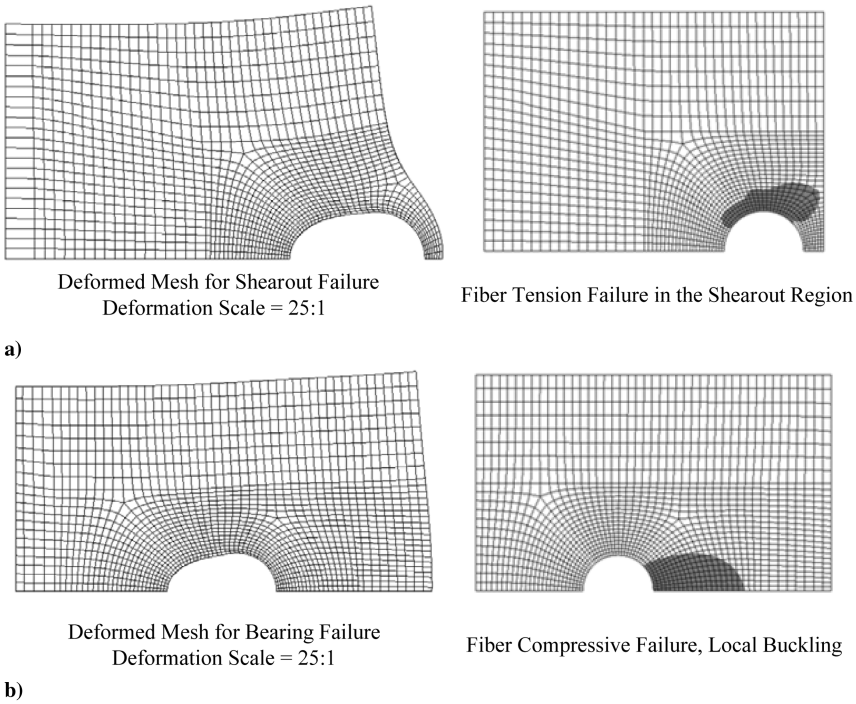

Fig. 13 Deformed finite element meshes and failure variables for a) shearout and b) bearing failure. Common contour scale, shaded areas represent Gauss points at which the failure criteria have been exceeded.

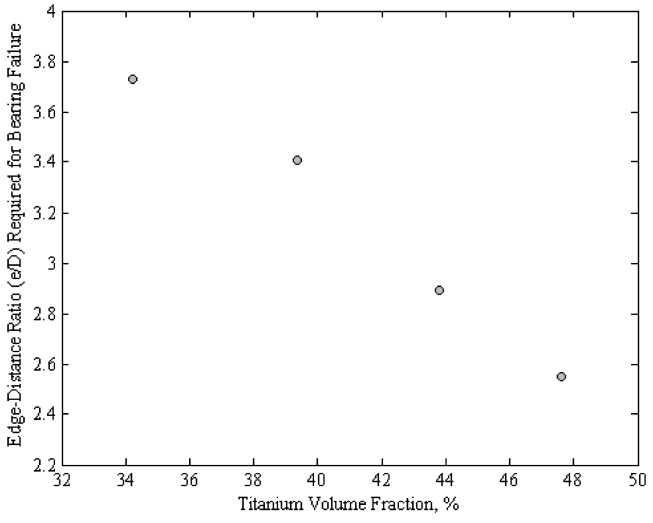

Fig. 14 Failure mode transition edge-distance ratio as a function of titanium content.

titanium content on the order of 35–50%. In this case, the ideal layup can be found from a failure mode vs volume fraction chart, such as that pictured in Fig. 14.

Acknowledgments

This work was supported by Raytheon Missile Systems with Robert Clark as the program monitor. The authors would like to Kenneth Mercer and Josh Jones of San Diego Composites for their helpful discussion of this work.

References

[1] Van Rooijen, R. G. J., Sinke, J., De Vries, T. J., and Van Der Zwaag, S., "Bearing Strength of Fiber Metal Laminates," *Journal of Composite Materials*, Vol. 40, No. 1, 2006, pp. 5–19. doi:10.1177/0021998305053509

[2] Wu, H. F., Wu, L. L., and Slagter, W. J., "Investigation on the Bearing Test Procedure for Fiber-Reinforced Aluminum Laminates," *Journal of Materials Science*, Vol. 29, No. 17, 1994, pp. 4592–4603. doi:10.1007/BF00376283

[3] Miller, J. L., Progar, D. J., Johnson, W. S., and St. Clair, T. L., "Preliminary Evaluation of Hybrid Titanium Composite Laminates," NASA TM-109095, 1994.

[4] Hagenbeek, M., Van Hengel, C., Bosker, O. J., and Vermeeren, C. A. J. R., "Static Properties of Fiber Metal Laminates," *Applied Composite Materials*, Vol. 10, Nos. 4–5, 2003, pp. 207–222. doi:10.1023/A:1025569316827

[5] Wu, G., and Yang, J. M., "Analytical Modelling and Numerical Simulation of the Nonlinear Deformation of Hybrid Fibre-Metal Laminates," *Modeling and Simulation in Materials Science and Engineering*, Vol. 13, No. 3, 2005, pp. 413–425 doi:10.1088/0965-0393/13/3/010.

[6] Sinke, J., "Development of Fibre Metal Laminates: Concurrent Multi-Scale Modeling and Testing," *Journal of Materials Science*, Vol. 41, No. 20, 2006, pp. 6777–6788. doi:10.1007/s10853-006-0206-5

[7] Greszczuk, L. B., "Stress Concentrations and Failure Criteria for Orthotropic and Anisotropic Plates with Circular Openings," *Composite Materials Testing and Design 2nd Conference*, American Society for Testing and Materials STP 497, Baltimore, MD, 1971, pp. 363–381.

[8] De Jong, T., "Stresses Around Pin-Loaded Holes in Elastically Orthotropic or Isotropic Laminates," *Journal of Composite Materials*, Vol. 11, No. 3, 1977, pp. 313–331. doi:10.1177/002199837701100306

[9] Military Handbook, *MIL-HDBK-5H: Metallic Materials and Elements for Aerospace Vehicle Structures*, Dept. of Defense, Washington, D.C., 1998.

[10] Hashin, Z., "Failure Criteria for Unidirectional Fiber Composites," *Journal of Applied Mechanics* Vol. 47, June 1980, pp. 329–335.

[11] Hibbitt, Karlsson, & Sorensen, Inc., *ABAQUS, A Finite Element System*, User's Manual, Ver. 6.6, 2006.

[12] Camanho, P. P., and Matthews, F. L., "Progressive Damage Model for Mechanically Fastened Joints in Composite Laminates," *Journal of Composite Materials*, Vol. 33, No. 12, 1999, pp. 2248–2280.

[13] Wu, P. S., and Sun, C. T., "Modeling Bearing Failure Initiation in Pin-Contact of Composite Laminates," *Mechanics of Materials*, Vol. 29, Nos. 3–4, 1998, pp. 325–335. doi:10.1016/S0167-6636(98)00019-2

[14] Hol, J., and Antonelli, V., "Progressive Damage Modeling of FMLs: Implementation in a UMAT Subroutine," *2003 ABAQUS User's Conference*, Simulia Systems, Providence, RI, 2003, pp. 1–11.

[15] Matzenmiller, A., Lubliner, J., and Taylor, R. L., "Constitutive Model for Anisotropic Damage in Fiber Composites," *Mechanics of Materials*, Vol. 20, No. 2, 1995, pp. 125–152. doi:10.1016/0167-6636(94)00053-0

[16] Linde, P., Pleitner, J., De Boer, H., and Carmone, C., "Modeling and Simulation of Fiber Metal Laminates," *2004 ABAQUS User's Conference*, Simulia Systems, Providence, RI, 2004, pp. 421–439.

[17] American Society for Testing and Materials, *Standard Test Method for Bearing Strength of Plastics, D953-92*, Annual Book of ASTM Standards, ASTM International, West Conshohocken, PA, 1992.

[18] American Society for Testing and Materials, *Standard Test Method for Bearing Response of Polymer Matrix Composite Laminates, D5961*, Annual Book of ASTM Standards, ASTM International, West Conshohocken, PA, 2005.

G. Schoeppner
Associate Editor